International Journal of Robotics and Control Systems
Vol. 6, No. 2, 2026, pp. 1164-1180
ISSN 2775-2658
http://pubs2.ascee.org/index.php/ijrcs

Sliding Mode Position Tracking Control-Based Waterwheel Plant Algorithm for Elbow Rehabilitation Systems

Attarid K. Ahmed [a,1,*], Laith K. Majeed [a,2], Saba Al-Wais [b,3], Huthaifa Al-Khazraji [a,4]

[a] College of Artificial Intelligence Engineering, University of Technology- Iraq, Baghdad, Iraq
[b] College of Biomedical Engineering, University of Technology-Iraq, Baghdad, Iraq
1 attarid.k.Ahmed@uotechnology.edu.iq; [2] laith.k.majeed@uotechnology.edu.iq; [3] saba.t.salim@uotechnology.edu.iq;
[4] huthaifa.k.ibrahim@uotechnology.edu.iq
* Corresponding Author

ARTICLE INFO

Article history
Received March 13, 2026
Revised April 08, 2026
Accepted April 18, 2026

Keywords
Elbow Rehabilitation System;
Sliding Mode Control;
Reaching Law;
Tracking Control;
Waterwheel Plant Algorithm;
MATLAB-Based Simulation;
Robust Analysis

ABSTRACT

Joint dysfunction affects millions of people worldwide, severely limiting their ability to carry out fundamental daily activities such as eating, drinking, and writing. These limitations often hinder independent self-care. To address this challenge, rehabilitation robots have been developed to assist individuals with physical impairments in performing daily tasks and preserving their autonomy. In this study, a sliding mode control (SMC) for position tracking of unit step and sinusoidal signal inputs of the elbow rehabilitation (Elb-Rehab) systems is proposed. In the context of performance enhancement of the SMC, two reaching laws are examined. The first reaching law is based on the hyperbolic tangent function (SMC_{tah}), whereas the second one is based on the saturation function (SMC_{sat}). SMC's designed parameters are tuned using the waterwheel plant algorithm (WPA) based on the integral of absolute error (IAE) as a cost function. Simulation experiments based on MATLAB software are used to examine the two control algorithms for the Elb-Rehab system, which are then analyzed. The simulation outcomes reveal that the tracking error based on the IAE of the system controlled by the SMC_{sat} is reduced by 12.68% and 76.3% compared to that of the system controlled by the SMC_{tah} for the unit step and sinusoidal signal inputs respectively. Furthermore, under an uncertainty scenario, the SMC_{sat} continues to outperform the SMC_{tah}. However, the SMC_{tah} shows slightly less sensitively to uncertainty than the SMC_{sat}.

1. Introduction

Every year, many people develop disabilities because their joints do not work properly. This can happen for different reasons, like getting older or having a stroke. For example, about 13.7 million new cases of stroke happen worldwide each year [1]. A lack of muscle control is commonly observed in these individuals because of difficulties in producing sufficient joint torque and in overcoming mechanical resistance at the joints. Such impairments significantly impair the ability to perform daily activities. Consequently, rehabilitation programs play a crucial role in regaining physical function and are integrated into everyday life [2], [3].

The rehabilitation process requires continuous involvement of medical professionals and specialists who must closely monitor each patient's movement. In conventional therapy, predefined exercises are manually assigned by a physician to individuals with disabilities to assess treatment progress throughout the rehabilitation period. Consequently, this approach is costly and time-consuming [4], [5]. The integration of wearable robotics technologies, particularly the elbow exoskeleton system, with an advanced control system can effectively address these challenges and enable improved rehabilitation outcomes.

Wearable exoskeletons enhance human performance by assisting human motions to reduce the user's effort and decrease fatigue [6]. Exoskeleton systems, as well as end effector systems, are patient-centric sports equipment and effector systems that provide in-depth control of joint angles and torques, making them an appropriate robotic modality for rehabilitative intervention in depth with severe motor impairment following brain injury. To perform their work, these exoskeleton technologies use flexible mechanical components that rely on actuators and sensor technology to perform their duties appropriately [7].

To guarantee the performance of exoskeleton systems for rehabilitation training, various control schemes have been developed. For instance, Three controllers, including proportional-integral (PI), fuzzy logic control (FLC), and sliding mode control (SMC), were presented by Jalani and Sadun [8], the results indicate that SMC provides superior control performance for the hand exoskeleton used in stroke rehabilitation, in terms of minimal overshoot, zero steady-state error, and the fastest settling time compared to PI and FLC controller. Nevertheless, the mathematical model is not described with sufficient clarity, and the paper does not analyze the impact of parameter variations on the system's behavior. Barbouch et al. successfully evaluated the efficacy of a feedback error learning algorithm in conjunction with SMC for elbow joint movements, utilizing a validated electrical simulation environment [9]. Brahim et al. [10] modeled a backstepping sliding-mode control scheme for tracking the predefined path of an ETSMARSE exoskeleton robot during passive therapy. The robotic device is intended for individuals with reduced upper-limb capabilities resulting from stroke. However, the process used to determine the control gains lacks clarity, making it difficult to assess the design methodology. Additionally, the study does not analyze the effect of parameter variations on system performance. A model-free back-stepping sliding-mode based control method was presented by Yang et al. [11]. An external back-stepping controller with a nonsingular quick output sliding controller is used to improve effectuality of the control. The overall uncertainties were resolved using time-delay prediction. In a comparable manner, a fractional SMC (FSMC) method to control a 7-DOF upper-limb exoskeleton was introduced by Islam et al. [12]. In their study, accurate kinematic modeling was not considered. The FSMC performs better than the SMC in terms of control signal monitoring and chattering.

Adaptive control has attracted extensive attention as an effective solution for exoskeleton systems. In this manner, Bembli et al. [13] designed an adaptive sliding-mode method that relies on gravitational correction to handle upper-limb exoskeleton systems subject to parameter constraints. A two-degree-of-freedom robotic system is used in a rehabilitation approach to aid in controlling the elbow and shoulder movements. Nguyen et al. [14] attempted to design an adaptive intelligent controller by integrating the fuzzy logic (FL) concept with conventional PID control, particularly on upper-limb exoskeleton robots where motor power is concentrated on pneumatic artificial muscles. PID controller compensates for approximation error and hysteresis, and the FL component approximates nonlinear equations. In a similar vein, an adaptable fuzzy neural network (AFNN) was developed by Liu et al. [15] to set elbow joint angles using sEMG. The AFNN demonstrated superior performance in both speed and precision compared to other neural network models, such as backpropagation and radial basis NN. Swarm optimization has been chosen by many researchers to find the optimal values of the tuning parameters of a controller [16]–[18]. For example, Waheed et al. [19] used particle swarm optimization (PSO) to improve back-stepping sliding mode control for elbow joint angles. The whale optimization algorithm (WOA) was used in [20] to improve the effectiveness

of SMC in the control of an elbow exoskeleton system. However, in these two studies, there is no analysis regarding the sensitivity of the results to parameter variations is provided.

Most of the previous studies do not evaluate the performance of the controller under uncertainty in the system parameters. Building on this, the current paper aims to explore SMC approach for position tracking of unit step and sinusoidal reference for the Elb-Rehab system taking into account the variation in the value of the viscous friction coefficient. Moreover, in the context of performance enhancement of the SMC, two reaching laws are examined. The first reaching law is based on the hyperbolic tangent function (SMC_{tah}), whereas the second one is based on the saturation function (SMC_{sat}). SMC's designed parameters are tuned using the waterwheel plant algorithm (WPA) based on the integral of absolute error (IAE) as a cost function. Simulation experiments based on MATLAB software are used to examine the two control algorithms for the Elb-Rehab system.

2. Mathematical Model

The elbow rehabilitation (Elb-Rehab) system is shown in Fig. 1. The device applies an actuator, which is used to help the patients in doing joint motions [19].

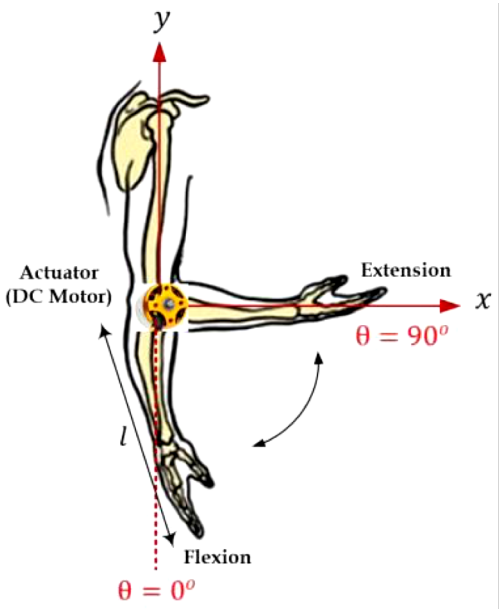

Fig. 1. Elb-rehab system

The biological arm and the Elb-Rehab dynamic model are developed in different ways. In this paper, the Lagrangian and Euler-Lagrange equations, as given in (1) and (2) respectively, are applied to establish the equations of motion [21].

$$L = E_k - E_g \tag{1}$$

$$\frac{d}{dt}\frac{\partial L}{\partial \dot{\theta}} - \frac{\partial L}{\partial \theta} = \tau_i \tag{2}$$

In (1), the system's kinetic (E_k) and gravitational (E_g) energies are expressed by the following equations as follows:

$$E_k = \frac{1}{2} I \dot{\theta}^2 \tag{3}$$

$$E_g = gml(1 - cos\,\theta) \tag{4}$$

In this expression, I signify the moment of inertia of the human elbow, and $m, g,$ and l refer to the mass, the acceleration of gravity, and the distance between the elbow joint and the centre of gravity, respectively. The moment of inertia is obtained according to (5) [13].

$$I = \frac{1}{2}ml^2 \tag{5}$$

Substitute (3), (4), and (5) into (1) get the following result:

$$L = \frac{1}{2}I\dot{\theta}^2 - gmI(1 - cos\,\theta) \tag{6}$$

In return to (2), τ_i is the input torque that is applied to the Elb-Rehab system, which is given by:

$$\tau_i = \tau_f + \tau_m \tag{7}$$

where the torques τ_f and τ_m are called the frictional and motor torque respectively. The torques τ_f and τ_m are given by:

$$\tau_f = K_v\dot{\theta} \tag{8}$$

$$\tau_m = I\ddot{\theta} + \tau_g\, sin\,\theta \tag{9}$$

Here, K_v represents the viscous friction coefficient, τ_g is the gravitational torque, and it is computed by (10) [18]:

$$\tau_g = gml \tag{10}$$

Substituting (8), (9), and (10) into (7) gives:

$$\tau_i = K_v\dot{\theta} + I\ddot{\theta} + \tau_g\, sin\,\theta \tag{11}$$

Rearrange (11) gives:

$$I\ddot{\theta} = \left(\frac{1}{I}\right)\left(-K_v\dot{\theta} - \tau_g\, sin\,\theta + \tau_i\right) \tag{12}$$

To end this, let us assume the angular position of the system $\theta = x_i$, the angular velocity of the system $\dot{\theta} = x_2$, and control input torque $\tau_i = u$, then, the mathematical model of the dynamic motion of the Elb-Rehab can be expressed using state variables as follows:

$$\dot{x}_1 = \dot{\theta} = x_2 \tag{13}$$

$$\dot{x}_2 = \ddot{\theta} = \frac{1}{I}\left(u - K_v x_2 - \tau_g sin(x_1)\right) \tag{14}$$

For the purpose of controlling design, (14) can be rewritten as follows:

$$\dot{x}_2 = f(X) + bu \tag{15}$$

where $f(X) = \frac{1}{I}\left(-K_v x_2 - \tau_g sin(x_1)\right)$ and $b = \frac{1}{I}$.

3. Sliding Mode Control Design

Feedback control has proven to be a remarkably engineering strategy for trajectory control because it continuously measures tracking errors and dynamically adjusts control inputs, ensuring

precise path following for a wide range of systems [22]–[27]. To address the disturbances and model uncertainties problem during tracking control, sliding mode control (SMC) is recommended as a method for controller design. It has two phases. The first phase is to define the surfaces that slide such that they meet the performance requirements. The next phase involves maintaining the system on the sliding surface [28]–[30].

Define the tracking error as:

$$e = x_d - x_1 \tag{16}$$

where x_1 is the angular position output and x_d is the desired angular position. Taking the first and the second derivative of e yields:

$$\dot{e} = \dot{x}_d - \dot{x}_1 = \dot{x}_d - x_2 \tag{17}$$

$$\ddot{e} = \ddot{x}_d - \dot{x}_2 \tag{18}$$

Substituting $\dot{x}_2$ from (15) into (18) obtains:

$$\ddot{e} = \ddot{x}_d - f(X) - bu \tag{19}$$

The trajectory of the sliding surface is chosen as follows:

$$s = \dot{e} + a_{smc}e \tag{20}$$

where $a_{smc} > 0$ is the tuning parameter. The results of the first derivation of s lead to $\dot{s} = \ddot{e} + a_{smc}e$. Substituting $\ddot{e}$ and $\dot{x}_2$ gives the following:

$$\dot{s} = \ddot{x}_d - f(X) - bu + a_{smc}\dot{e} \tag{21}$$

The second part of the SMC control law deals with switching control, which appears as a discontinuous element that drives the system to slide along a predefined surface [31], [32]. For the system to stay on this surface, the derivative of the sliding surface must match the reaching law (RL). In other words, the RL is the rule that defines how the system states are driven toward the sliding surface. Therefore, selecting an appropriate RL is crucial to minimizing the chattering effect commonly associated with SMC. In this paper, two RLs are proposed. The first RL is based on the hyperbolic tangent (tanh) function and is given by [33], [34]:

$$\dot{s} = -k_{tah}\left(\frac{2}{\pi}\right)tanh(\beta s) \tag{22}$$

where k_{tah} is a tuning parameter, which is a strictly positive number, where $tanh\, s$ is given by:

$$tanh\, s = \frac{e^s - e^{-s}}{e^s + e^{-s}} \tag{23}$$

Based on this RL, the control u_{tah} is obtained by setting (21) equal to (22), and accordingly, (24) is obtained as follows:

$$\ddot{x}_d - F(x,t) - u_{tah} + a_{tah}\dot{e} = -k_{tah}\left(\frac{2}{\pi}\right)tanh\, s \tag{24}$$

Rearrange (24) to find u_{tah}:

$$u_{tah} = \ddot{x}_d - F(x,t) + a_{tah}\dot{e} + k_{tah}\left(\frac{2}{\pi}\right)tanh\, s \tag{25}$$

The second RL is based on the saturation (sat) function, and it is given by [35], [36]:

$$\dot{s} = -k_{sat} sat(s/\emptyset) \tag{26}$$

where k_{sat} is an adjusted parameter > 0, $sat(s/\emptyset)$ is given by:

$$\text{sat}\left(\frac{s}{\emptyset}\right) = \begin{cases} +1 & \text{if } \frac{s}{\emptyset} > 0 \\ \frac{s}{\emptyset} & \text{if } -1 < \frac{s}{\emptyset} < 1 \\ -1 & \text{if} \frac{s}{\emptyset} < 0 \end{cases} \tag{27}$$

The control law for this RL u_{sat} is given by putting (21) and is equal to (26) as given:

$$\ddot{x}_d - f(X) - bu_{sat} + a_{sat}\dot{e} = -k_{sat} sat(s/\emptyset) \tag{28}$$

Rearrange (28) to find u_{sat}:

$$u_{sat} = \ddot{x}_d - F(x,t) + a_{sat}\dot{e} + k_{sat} sat\left(\frac{s}{\emptyset}\right) \tag{29}$$

4. Waterwheel Plant Algorithm

The aim of optimization algorithms is to determine the optimal set of decision variables that either maximizes or minimizes a given objective function. Owing to their simplicity and adaptability, and inspired by the collective behavior and hunting strategies of animals, many swarm-based algorithms have been successfully developed and applied to solve complex problems [37]–[41]. Based on that, the swarm optimization techniques have been widely employed to obtain optimal controller parameters rather than the classical trial-and-error approaches [42]–[52]. The Waterwheel Plant Algorithm (WPA) was proposed by Abdelhamid et al. in 2023 [53]. The algorithm draws inspiration from the natural hunting behavior of the carnivorous waterwheel plant, also known as Aldrovanda vesiculosa [54]. The core concept is based on a mathematical simulation of the plant's hunting behavior—namely, prey detection, capture, and relocation for consumption—which underpins the optimization process's exploration and exploitation mechanisms. The WPA is an iterative optimization based on population search capability, depending on the population members, to find an optimization solution. Each member of the population can propose a potential solution to the optimization challenge, which is referred to as a 'water wheel.' The algorithm is inspired by the natural hunting strategy of the water wheel plant, which relies on its strong sense of smell to locate insects, capturing them, and then transferring the prey to its feeding tube. IN the following section, the WPA mathematical model is explained to address optimization challenges and mimic the plant's hunting strategy, consisting of an initial setup stage and two main stages: exploration and exploitation.

4.1. Initialization Stage

The algorithm initializes a population of 'waterwheels' representing candidate solutions. The population is organized in matrix form, where each vector corresponds to a waterwheel in the search space. The initial positions are randomly generated within the problem's defined upper and lower bounds of the problem. This initialization marks the start of the optimization process [53].

- **Population matrix (P):** this matrix contains the position of all N waterwheels for m problem variables.
- **Initial position $L_{i,j}$:** the position of the *i-th* waterwheel in the *j-th* dimension is initialized using the following formula:

$$L_{i,j} = lb_j + r_{i,j}(ub_j - lb_j); \quad i = 1, 2, 3, \dots, N; \quad j = 1, 2, 3, \dots, m$$

where $r_{i,j}$ is a random number in the interval $[0, 1]$; lb_j and ub_j are the lower bound and upper bound of the *j-th* problem variable, respectively.

- **Objective function (F):** the fitness of each waterwheel (solution) is determined by the objective function and recorded in a vector.

4.2. Exploration Stage

The waterwheel plant's behavior inspires the fundamental ideal at this stage for detecting and attacking insects, characterized by significant movement. To enhance exploration of the search space, the agents undergo significant positional changes. The search agents' positions are updated using equations designed to encourage wider exploration of the search domain. The update equation is considered effective only when the new position yields a better solution [55].

$$\vec{\psi} = \vec{r_1} \cdot \left(\vec{L}(t) + 2M\right) \tag{30}$$

$$\vec{L}(t+1) = \vec{L}(t) + \vec{\psi}(2M + \vec{r_2}) \tag{31}$$

where $\vec{r_1}$ and $\vec{r_2}$ are random variables with values in the ranges [0, 2] and [0, 1], respectively. In addition, M is an exponential variable with values in the range [0, 1], and $\vec{\psi}$ is a vector that indicates the diameter of the circle in which the waterwheel plant searches for promising areas. If no improvement is seen after three iterations, a Gaussian mutation is applied to prompt exploration of a new region.

$$\vec{L}(t+1) = Gaussion(\mu\rho, \sigma) + \vec{r_1} \cdot \left(\frac{\vec{L}(t) + 2M}{\vec{\psi}}\right) \tag{32}$$

The exploration phase facilitates a thorough search, enabling the algorithm to scan a wide area of the search space, detect promising regions, and avoid becoming trapped in local optima.

4.3. Exploitation Stage

This phase is modeled after the plant capturing an insect and transporting it to a feeding tube, which involves smaller, more controlled movements. It leads to small changes in the position of the waterwheels, allowing fine-tuning of the solution. The update equations are designed to make smaller adjustments relative to the current position and the best-known solution (L_{best}), guiding the search toward the current optimum. The waterwheel moves according to these equations [56]:

$$\vec{\psi} = \vec{r_3} \cdot \left(M\vec{L}_{best}(t)\right) + r_3\vec{L}(t) \tag{33}$$

$$\vec{L}(t+1) = \vec{L}(t) + M\vec{\psi} \tag{34}$$

where $\vec{r_3}$ is a random variable with values in the range [0, 2], $\vec{L}(t)$ is the current solution at iteration t, and $\vec{L}_{best}(t)$ is the best solution.

If the solution stagnates, a sine-based mutation is used for a controlled local adjustment [57].

$$\vec{L}(t+1) = (\vec{r_1} + M)\, sin\left(\frac{F}{C}\theta\right) \tag{35}$$

where F and C are random variables with values in the range [−5, 5]. In addition, the value of M decreases exponentially using the following equation:

$$M = \left(1 + \frac{2 * t^2}{T_{max}} + F\right) \tag{36}$$

The main objective of the exploitation phase is to perform a local search. Once a promising region is identified, this phase refines the search within that area to converge upon a better, more precise solution.

5. Results and Discussion

In this section, the computer simulation is given to evaluate the proposed controller (the SMC_{sat} and the SMC_{tah}) for tracking trajectory control system for the Elb-Rehab system. MATLAB software was utilized to perform the numerical simulation. Table 1 lists the numerical value of the physical element of the Elb-Rehab system. Two desired trajectory are used in simulation. The first one is a unit step input whereas the second one is a composite sinusoidal signal containing multiple frequency components, as defined by:

$$x_r = sin(2t) + sin(5t) \tag{37}$$

Table 1. Model physical specifications

Parameters	Value
Length (l)	0.24 m
Mass (M)	1.55 kg
gravity acceleration(g)	9.81 m/s2
Viscous friction coefficient (kv)	1.5 Nm/(rad/s)

The cost function used by the WPA, namely the integral of absolute error (IAE), was chosen to achieve optimal performance of the SMC_{sat} and the SMC_{tah}. This IAE is given by [58]–[60]:

$$IAE = \int_0^{t_{sim}} |e|\, dt \tag{38}$$

where t_{sim} refers to the simulation duration, and e is the tracking error, which obtained by the difference between the angular position of the wearable exoskeleton and the required angular position. The configurations of the the SMC_{sat} and the SMC_{tah} optimized by WPA for the Elb-Rehab system are shown in Fig. 2 and Fig. 3. Table 2 shows the values for the design parameters of the SMC_{sat} and the SMC_{tah}.

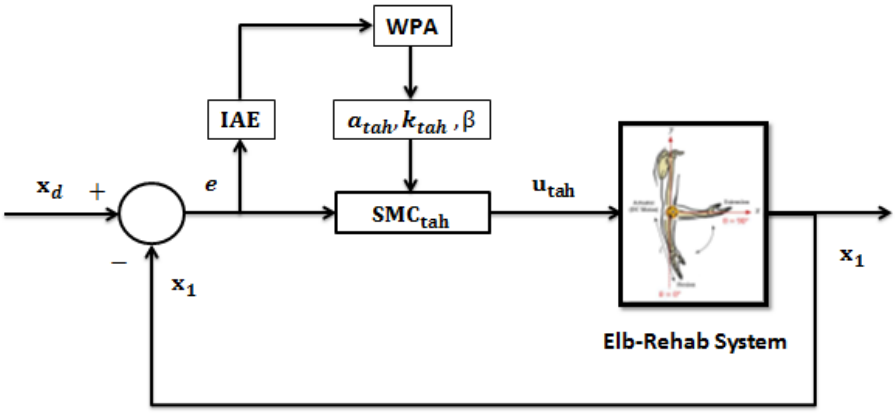

Fig. 2. SMC_{sat} based WPA for the Elb-Rehab system

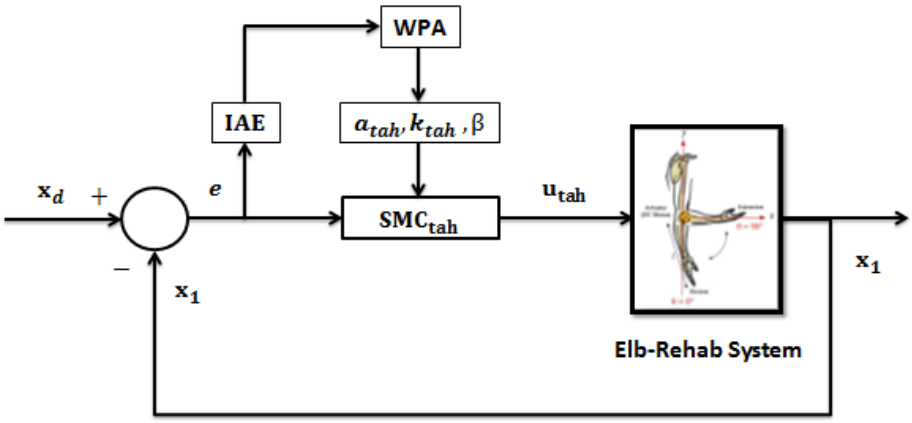

Fig. 3. SMC_{tah} based WPA for Elb-Rehab system

Table 2. Optimal value of configuration parameters

Controller	Parameters	Values
SMC_{sat}	a_{sat}	33.8
	k_{sat}	168.7
	Φ	0.32
SMC_{tah}	a_{tah}	35.4
	k_{tah}	220.3
	β	0.81

5.1. Normal Operation

This simulation is to evaluate the performance of the SMC_{sat} and the SMC_{tah} in normal operation. Fig. 4 and Fig. 5 show the output position response and the tracking position error for the unit step input. Table 3 shows the numerical value result for the IAE index. Based on Fig. 4 and with the help of the visualization of the tracking error in Fig. 5, it can be seen that the SMC_{sat} outperforms the SMC_{tah}. This finding can be proven numerically using Table 3, which undoubtedly shows that the value of the IAE (1.79) for SMC_{sat} is significantly less than the value of the IAE (2.05) for the SMC_{tah}.

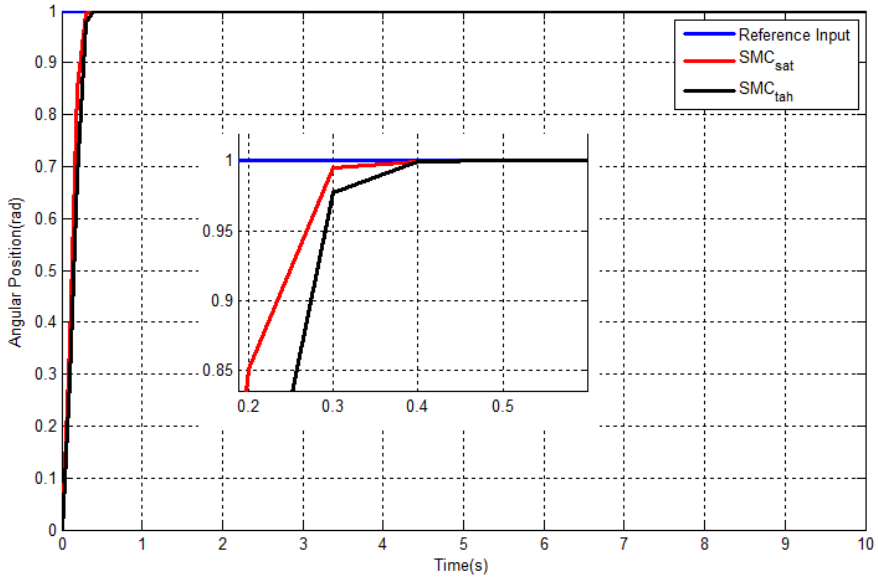

Fig. 4. System response of SMC_{sat} and SMC_{tah} under normal operation (unit step input)

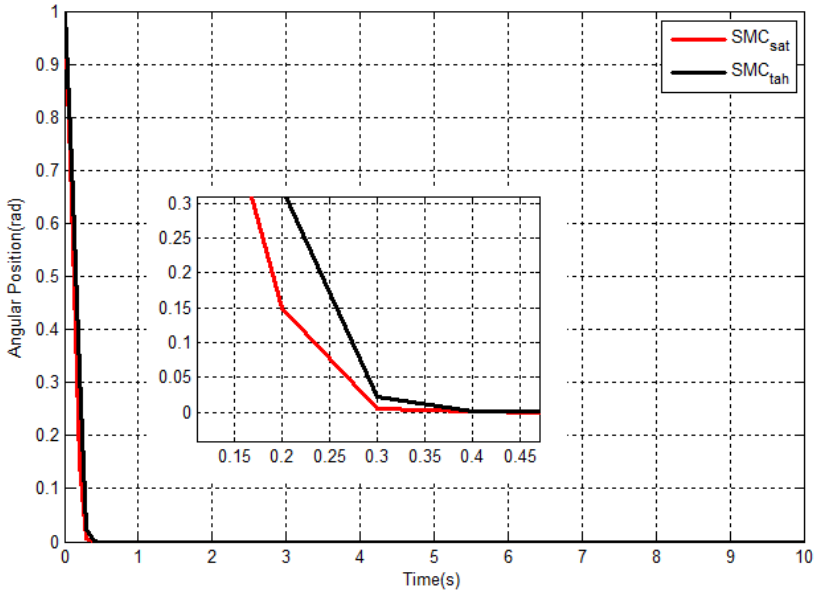

Fig. 5. Tracking error of SMC_{sat} and SMC_{tah} under normal operation (unit step input)

Table 3. Comparison of dynamic performance under normal operation (unit step input)

Performance	SMC_{sat}	SMC_{tah}
IAE (rad)	1.79	2.05

Moreover, Fig. 6 and Fig. 7 show the output position response and the tracking position error for the sinusoidal signal input. Table 4 shows the numerical value result for the IAE index. Based on Fig. 6 and with the help of the visualization of the tracking error in Fig. 7, it can be seen that the SMC_{sat} outperforms the SMC_{tah}. This finding can be proven numerically using Table 4, which shows that the value of the IAE (0.095) for SMC_{sat} is significantly less than the value of the IAE (0.402) for the SMC_{tah}.

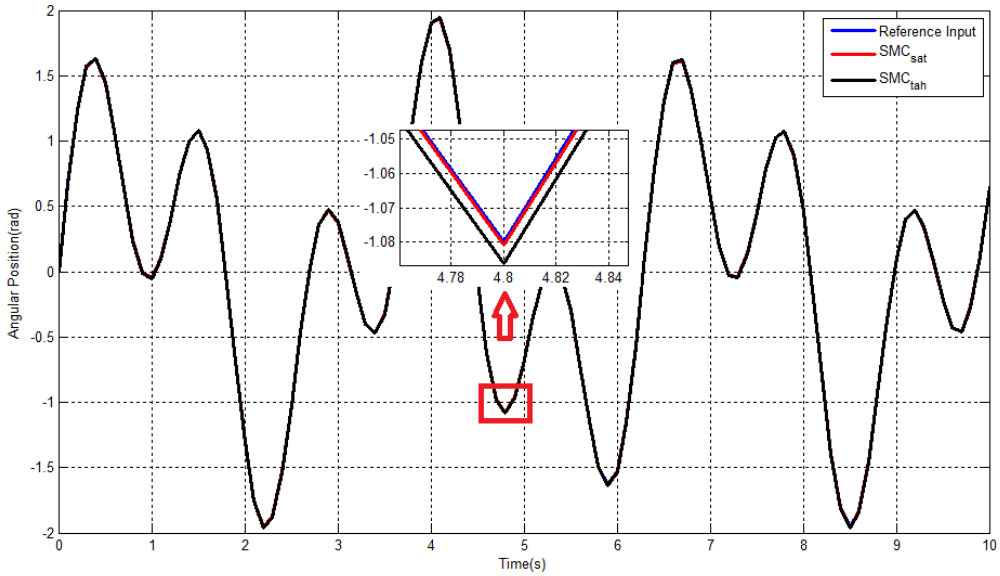

Fig. 6. System response of SMC_{sat} and SMC_{tah} under normal operation (sinusoidal signal input)

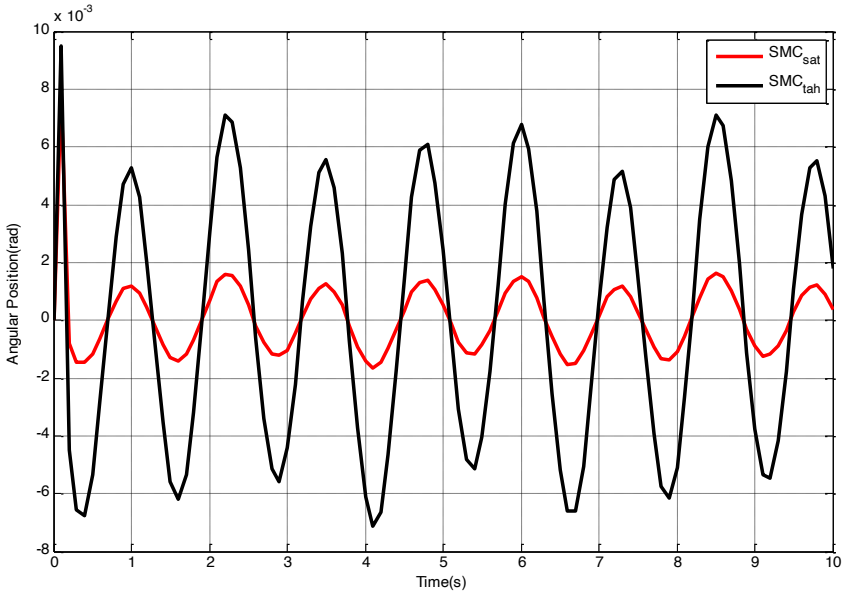

Fig. 7. Tracking error of SMC_{sat} and SMC_{tah} under normal operation (sinusoidal signal input)

Table 4. Comparison of dynamic performance under normal operation

Performance	SMC_{sat}	SMC_{tah}
IAE (rad)	0.095	0.402

5.2. Uncertainty

To examine the resilience of the two controllers against uncertainty, it was assumed that the viscous friction coefficient (K_v) is increased by 30% of its value. Fig. 8 and Fig. 9 show the response and tracking error of the two controlled systems for the unit step input.

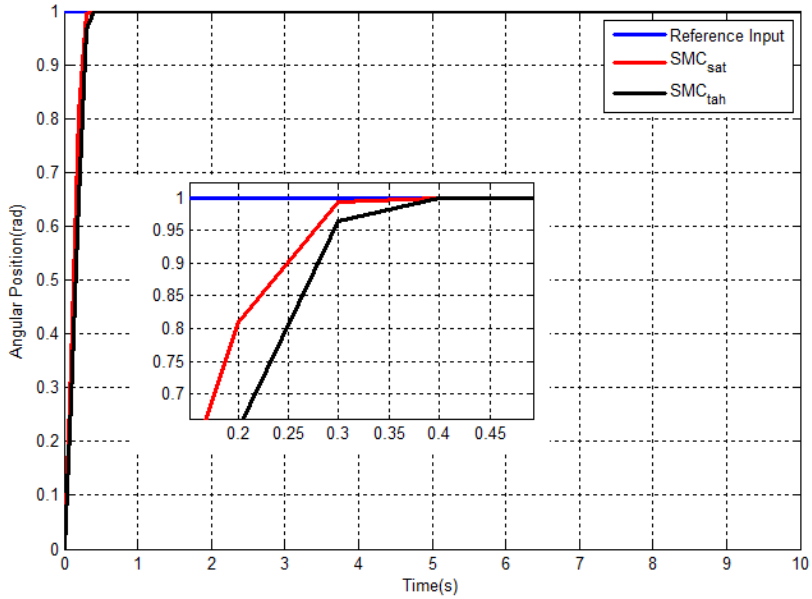

Fig. 8. System response of SMC_{sat} and SMC_{tah} under uncertainty (unit step input)

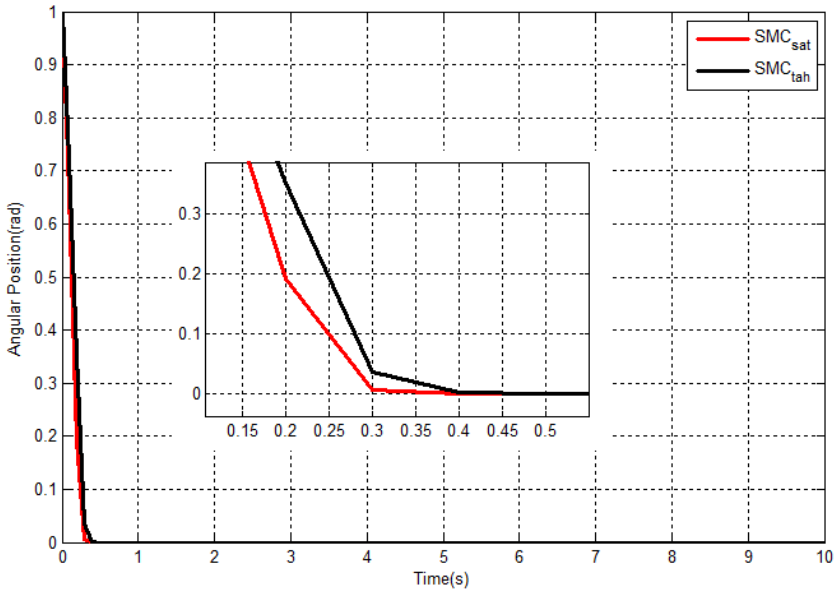

Fig. 9. Tracking error of SMC_{sat} and SMC_{tah} under uncertainty (unit step input)

Table 5 contains the associated numerical values of the IAE. It can be seen that while SMC_{sat} ($IAE = 1.85$) is outperform SMC_{tah} ($IAE = 2.11$) under uncertain conditions. However, the changing in the magnitude of its performance indicates that the SMC_{sat} has higher sensitivity to uncertainty compared to SMC_{tah}. Based on the results, it can be observed that the IAE for the SMC_{tah} was 2.05 in normal operation and it became 2.11 under uncertainty (increased by 2.84%) whereas the IAE for the SMC_{sat} was 1.79 in normal operation and it became 1.85 (increased by 3.24%). These results reveal that SMC_{tah} has slightly more robustness characteristic than SMC_{sat}.

Table 5. Comparison of dynamic performance under normal operation (unit step input)

Performance	SMC_{sat}	SMC_{tah}
IAE (rad)	1.85	2.11

Moreover, Fig. 10 and Fig. 11 show the response and tracking error of the two controlled systems for the sinusoidal signal input.

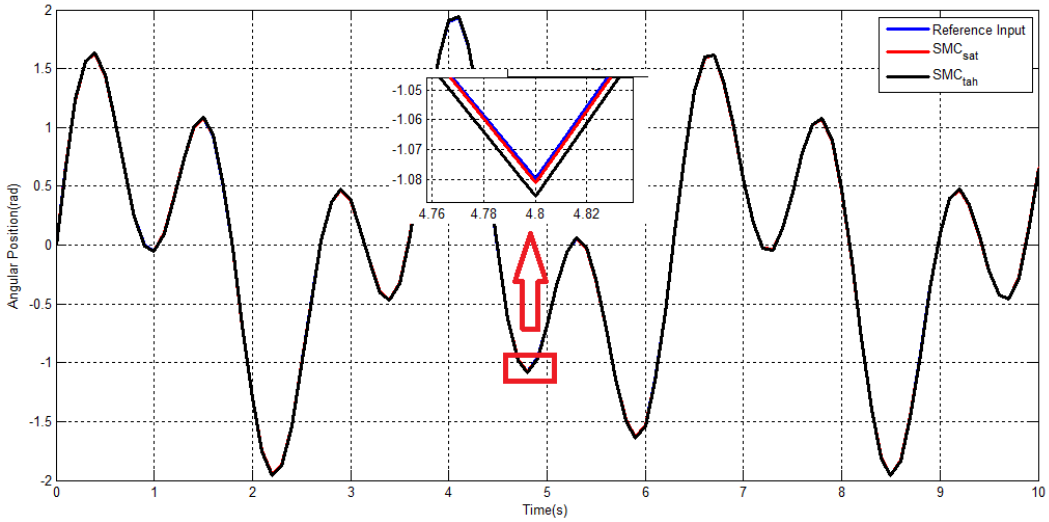

Fig. 10. System response of SMC_{sat} and SMC_{tah} under uncertainty (sinusoidal signal input)

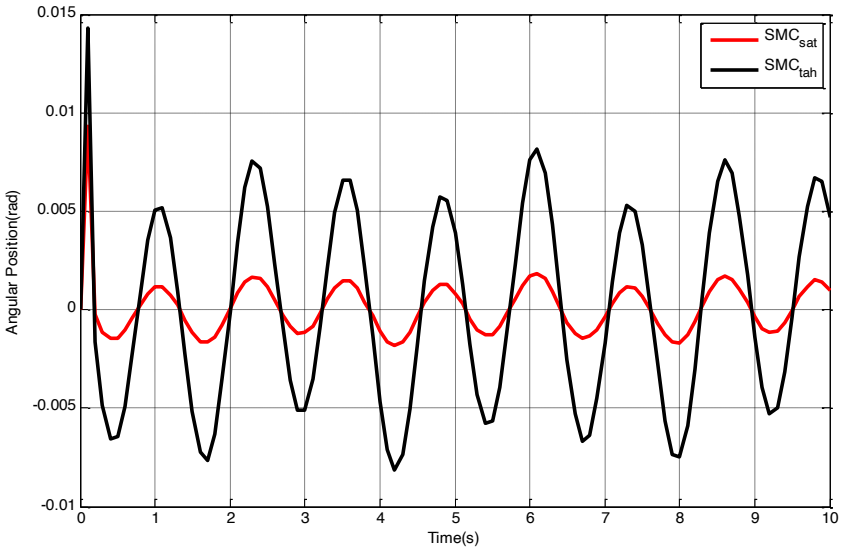

Fig. 11. Tracking error of SMC_{sat} and SMC_{tah} under uncertainty (sinusoidal signal input)

Table 6 contains the associated numerical values of the IAE. It can be seen that while SMC_{sat} ($IAE = 0.105$) continues to outperform SMC_{tah} ($IAE = 0.442$) under uncertain conditions, the magnitude of its performance degradation indicates a higher sensitivity to uncertainty compared to SMC_{sat}. Based on the results, it can be observed that the IAE for the SMC_{tah} was 0.402 in normal operation and it became 0.443 under uncertainty (increased by 9.04%) whereas the IAE for the SMC_{sat} was 0.095 in normal operation and it became 0.105 (increased by 9.52%). These results reveal that SMC_{tah} has slightly more robustness characteristic than SMC_{sat}.

Table 6. Comparison of dynamic performance under uncertainty

Performance	SMC_{sat}	SMC_{tah}
IAE (rad)	0.105	0.442

6. Conclusion

This paper presents the design of a position tracking control scheme for elbow rehabilitation (Elb-Rehab) systems utilizing the sliding mode control (SMC) methodology. The control law of the SMC is obtained based on two reaching laws, hyperbolic tangent function (SMC_{tah}) and the saturation function (SMC_{sat}). The waterwheel plant algorithm (WPA) was applied to tune the design parameters of both the SMCtah and the SMC_{sat}, to further enhance the controlled system. The results under normal operation demonstrate that SMC_{sat} outperforms SMC_{tah} in controlling the Elb-Rehab system. The SMC_{sat} exhibits the fastest tracking response to the desired tracking output. Under parametric uncertainty, the SMC_{sat} remains better in performance than SMC_{tah}. Howerver, the latter show slightly less sensitive to such variations

It is important to acknowledge several limitations of the present study. Specifically, the results are based solely on MATLAB simulations without experimental or hardware validation. Besides, the actuator model considered is simplified. These limitations may affect the generalizability and practical applicability of the findings. Therefore, future work will focus on implementing hardware-based validation and developing more realistic actuator models to enhance the robustness of the proposed approach.

Author Contribution: All authors contributed equally to the main contributor to this paper. All authors read and approved the final paper.

Funding: This research received no external funding.

Conflicts of Interest: The authors declare no conflict of interest.

References

[1] J. Miguel-Fernández, J. Lobo-Prat, E. Prinsen, J. Font-Llagunes, and L. Marchal-Crespo, "Control strategies used in lower limb exoskeletons for gait rehabilitation after brain injury: A systematic review and analysis of clinical effectiveness," *Journal of NeuroEngineering and Rehabilitation*, vol. 20, no. 1, p. 23, 2023, https://doi.org/10.1186/s12984-023-01144-5.

[2] F. J. Badesa, R. Morales, N. Garcia-Aracil, J. M. Sabater, A. Casals, and L. Zollo, "Auto-adaptive robot-aided therapy using machine learning techniques," *Computer Methods and Programs in Biomedicine*, vol. 116, no. 2, pp. 123–130, 2014, https://doi.org/10.1016/j.cmpb.2013.09.011.

[3] M. R. Islam, M. Assad-Uz-Zaman, B. Brahmi, Y. Bouteraa, I. Wang, and M. H. Rahman, "Design and development of an upper limb rehabilitative robot with dual functionality," *Micromachines*, vol. 12, no. 8, p. 870, 2021, https://doi.org/10.3390/mi12080870.

[4] S. M. Mahdi, N. Q. Yousif, A. A. Oglah, M. E. Sadiq, A. J. Humaidi, and A. T. Azar, "Adaptive synergetic motion control for wearable knee-assistive system: A rehabilitation of disabled patients," *Actuators*, vol. 11, no. 7, p. 176, 2022, https://doi.org/10.3390/act11070176.

[5] A. Zahedi, Y. Wang, U. Martinez-Hernandez, and D. Zhang, "A wearable elbow exoskeleton for tremor suppression equipped with rotational semi-active actuator," *Mechanical Systems and Signal Processing*, vol. 157, p. 107674, 2021, https://doi.org/10.1016/j.ymssp.2021.107674.

[6] A. Nasr, S. Bell, and J. McPhee, "Optimal design of active-passive shoulder exoskeletons: A computational modeling of human-robot interaction," *Multibody System Dynamics*, vol. 57, no. 1, pp. 73–106, 2023, https://doi.org/10.1007/s11044-022-09855-8.

[7] H. Herr, "Exoskeletons and orthoses: Classification, design challenges and future directions," *Journal of NeuroEngineering and Rehabilitation*, vol. 6, no. 21, pp. 1–9, 2009, https://doi.org/10.1186/1743-0003-6-21.

[8] J. Jalani and A. S. Sadun, "Optimizing control strategies for hand exoskeleton: A comparative study of controllers," *International Journal of Integrated Engineering*, vol. 17, no. 1, pp. 401–415, 2025, https://doi.org/10.30880/ijie.2025.17.01.033.

[9] H. Barbouch, F. Resquin, J. Gonzalez-Vargas, N. K. Haddad, and S. Belghith, "Feedback error learning with sliding mode control for functional electrical stimulation elbow joint simulation," *International Journal of Innovative Technology and Exploring Engineering*, vol. 8, no. 12, pp. 2971–2982, Oct. 2019, https://doi.org/10.35940/ijitee.K2026.1081219.

[10] B. Brahmi, M. Rahman, M. Saad, C. O. Luna, and M. R. Islam, "Sliding mode-backstepping control for upper-limb rehabilitation with the ETS-MARSE exoskeleton robot," in *RESNA Conference*, Arlington, VA, USA, Jun. 2016, pp. 1–7, https://www.resna.org/sites/default/files/conference/2016/pdf_versions/emerging_tech/brahim.pdf.

[11] P. Yang, J. Sun, J. Wang, G. Zhang, and Y. Zhang, "Model-free based back-stepping sliding mode control for wearable exoskeletons," in *Proceedings of the 2019 25th International Conference on Automation and Computing (ICAC)*, 2019, pp. 1–6, https://doi.org/10.23919/IConAC.2019.8895069.

[12] M. R. Islam, M. Rahmani, and M. H. Rahman, "A novel exoskeleton with fractional sliding mode control for upper limb rehabilitation," *Robotica*, vol. 38, no. 11, pp. 2099–2120, 2020, https://doi.org/10.1017/S0263574719001851.

[13] S. Bembli, N. K. Haddad, and S. Belghith, "Adaptive sliding mode control with gravity compensation: Application to an upper-limb exoskeleton system," in *MATEC Web of Conferences*, vol. 261, 2019, p. 06001, https://doi.org/10.1051/matecconf/201926106001.

[14] H. T. Nguyen, V. C. Trinh, and T. D. Le, "An adaptive fast terminal sliding mode controller of exercise-assisted robotic arm for elbow joint rehabilitation featuring pneumatic artificial muscle actuator," *Actuators*, vol. 9, no. 4, p. 118, Nov. 2020, https://doi.org/10.3390/act9040118.

[15] Y. Liu, C. Li, Z. Teng, K. Liu, G. Wang, and Z. Sun, "Intention recognition of elbow joint based on sEMG using adaptive fuzzy neural network," in *Proceedings of the 2020 5th International Conference on Mechanical, Control and Computer Engineering (ICMCCE)*, Harbin, China, 2020, pp. 1091–1096, https://doi.org/10.1109/ICMCCE51767.2020.00240.

[16] F. R. Yaseen, M. Q. Kadhim, H. Al-Khazraji, and A. J. Humaidi, "Decentralized control design for heating system in multi-zone buildings based on whale optimization algorithm," *Journal Européen des Systèmes Automatisés*, vol. 57, no. 4, pp. 981–989, 2024, https://doi.org/10.18280/jesa.570406.

[17] D. Z. Mohamed, H. Al-Khazraji, R. Al-Majeez, A. F. Hassan, and A. J. Humaidi, "Multi-verse optimizer based classical and nonlinear PI controller design for TCP/AQM system: A comparative study," *Mathematical Modelling of Engineering Problems*, vol. 12, no. 10, pp. 3461–3467, 2025, https://doi.org/10.18280/mmep.121012.

[18] F. R. Al-Ani, O. F. Lutfy, and H. Al-Khazraji, "Optimal synergetic and feedback linearization controllers design for magnetic levitation systems: A comparative study," *Journal of Robotics and Control*, vol. 6, no. 1, pp. 22–30, 2025, https://doi.org/10.18196/jrc.v6i1.24452.

[19] Z. A. Waheed and A. J. Humaidi, "Design of optimal sliding mode control of elbow wearable exoskeleton system based on whale optimization algorithm," *Journal Européen des Systèmes Automatisés*, vol. 55, no. 4, p. 459, 2022, https://doi.org/10.18280/jesa.550404.

[20] Z. A. Waheed, A. J. Humaidi, M. E. Sadiq, A. A. Al-Qassar, A. F. Hasan, A. Q. Al-Dujaili, A. R. Ajel, and S. J. Abbas, "Control of elbow rehabilitation system based on optimal-tuned backstepping sliding mode controller," *Journal of Engineering Science and Technology*, vol. 18, no. 1, pp. 584–603, 2023, https://jestec.taylors.edu.my/Vol%2018%20Issue%201%20February%20%202023/18_1_38.pdf.

[21] K. Al-Badri, H. Dulaimi, H. Al-Khazraji, and A. J. Humaidi, "Adaptive neural network control for load-varying two-link robots using honey badger optimization," *Journal of Robotics and Control (JRC)*, vol. 6, no. 2, pp. 1061–1068, 2025, https://doi.org/10.18196/jrc.v6i2.26370.

[22] N. W. Madebo, C. M. Abdissa, and L. N. Lemma, "Enhanced trajectory control of quadrotor UAV using fuzzy PID-based recurrent neural network controller," *IEEE Access*, vol. 12, pp. 190454–190469, 2024, https://doi.org/10.1109/ACCESS.2024.3516494.

[23] A. K. Ahmed, H. Al-Khazraji, O. F. Lutfy, and A. S. Al-Araji, "Comparative analysis of control strategies for tracking periodic sinusoidal references in magnetic levitation systems," *International Journal of Robotics & Control Systems*, vol. 5, no. 4, pp. 2325–2343, 2025, https://pubs2.ascee.org/index.php/IJRCS/article/view/2116.

[24] Z. Bingul and K. Gul, "Intelligent PID with PD feedforward trajectory tracking control of an autonomous underwater vehicle," *Machines*, vol. 11, no. 2, p. 300, 2023, https://doi.org/10.3390/machines11020300.

[25] H. D. Long and V. X. Duc, "Enhanced disturbance estimation for tracking control of nonlinear systems using adaptive fuzzy finite-time observers," *Journal of Fuzzy Systems and Control*, vol. 3, no. 3, pp. 250–258, 2025, https://ejournal.ptti.web.id/index.php/jfsc/article/view/348.

[26] E. Okafor, D. Udekwe, Y. Ibrahim, M. B. Mu'azu, and E. G. Okafor, "Heuristic and deep reinforcement learning-based PID control of trajectory tracking in a ball-and-plate system," *Journal of Information and Telecommunication*, vol. 5, no. 2, pp. 179–196, 2021, https://doi.org/10.1080/24751839.2020.1833137.

[27] F. R. Al-Ani, O. F. Lutfy, and H. Al-Khazraji, "Optimal backstepping and feedback linearization controllers design for tracking control of magnetic levitation system: A comparative study," *Journal of Robotics and Control (JRC)*, vol. 5, no. 6, pp. 1888–1896, 2024, https://journal.umy.ac.id/index.php/jrc/article/view/24073.

[28] F. Haroon, M. Aamir, A. Waqar, S. M. Qaisar, S. U. Ali, and A. T. Almaktoom, "A composite exponential reaching law-based SMC with rotating sliding surface selection mechanism for two-level three-phase VSI in vehicle-to-load applications," *Energies*, vol. 16, no. 1, p. 346, 2023, https://doi.org/10.3390/en16010346.

[29] M. Cengiz and T. Duman, "Sliding mode control for a single-phase grid-connected H-bridge NPC inverter with a symmetrical LCL filter," *Computers and Electrical Engineering*, vol. 117, p. 109298, 2024, https://doi.org/10.1016/j.compeleceng.2024.109298.

[30] K. Cherif, A. Sahbani, and K. B. Saad, "Performance evaluation of PI and sliding mode control for PMSM in electric vehicle applications," *Engineering, Technology & Applied Science Research*, vol. 14, no. 4, pp. 15464–15470, 2024, https://doi.org/10.48084/etasr.7172.

[31] N. Qiao, L. Wang, M. Liu, and Z. Wang, "Sliding mode controller with improved reaching law for harvesting robots," *Journal of Intelligent & Robotic Systems*, vol. 104, no. 1, p. 9, 2022, https://doi.org/10.1007/s10846-021-01536-6.

[32] J. W. Chan, "Sliding mode control of brushless DC motor speed control," *Malaysian Journal of Science and Advanced Technology*, vol. 2, no. 4, pp. 188–193, 2022, https://doi.org/10.56532/mjsat.v2i4.57.

[33] A. F. Hasan, M. Nawfal, A. S. Al-Araji, H. Al-Khazraji, and A. J. Humaidi, "Improved sliding mode control for maximum power point tracking in solar photovoltaic applications under varying conditions," *International Journal of Robotics and Control Systems*, vol. 5, no. 3, pp. 1790–1807, 2025, https://doi.org/10.31763/ijrcs.v5i3.1925.

[34] J. Gu and S. Pan, "Sliding mode control of dual active bridge converter based on hyperbolic tangent function," in *Journal of Physics: Conference Series*, vol. 2803, no. 1, p. 012050, 2024, https://doi.org/10.1088/1742-6596/2803/1/012050.

[35] A. M. Hameed and A. K. Hamoudi, "A 2-link robot with adaptive sliding mode controlled by barrier function," *Journal Européen des Systèmes Automatisés*, vol. 56, no. 6, p. 1105, 2023, https://doi.org/10.18280/jesa.560620.

[36] A. A. Ebrahim, "Modeling of a sliding mode controller to control the tracking system for solar panels with two degrees of freedom," *Control Systems and Optimization Letters*, vol. 4, no. 1, pp. 91–100, 2026, https://ejournal.csol.or.id/index.php/csol/article/view/277.

[37] X. S. Yang, "Nature-inspired optimization algorithms: Challenges and open problems," *Journal of Computational Science*, vol. 46, p. 101104, 2020, https://doi.org/10.1016/j.jocs.2020.101104.

[38] A. Uzzaman, M. Islam, and S. Ahmed, "Bio-inspired hybrid control for autonomous vehicles: Improving real-time navigation through the integration of ACO and PSO," *Control Systems and Optimization Letters*, vol. 3, no. 3, pp. 234–240, 2025, https://ejournal.csol.or.id/index.php/csol/article/view/204.

[39] S. Khlil, H. Al-Khazraji, and Z. Alabacy, "Solving assembly production line balancing problem using greedy heuristic method," in *IOP Conference Series: Materials Science and Engineering*, vol. 745, no. 1, p. 012068, 2020, https://doi.org/10.1088/1757-899X/745/1/012068.

[40] A. I. Abdulkareem, H. A. Dhahad, and N. Q. Yousif, "Prospect theory in particle swarm optimization for constrained nonlinear optimization problems," in *2018 Third Scientific Conference of Electrical Engineering (SCEE)*, Dec. 2018, pp. 144–149, https://doi.org/10.1109/SCEE.2018.8684144.

[41] A. Dafid, A. I. Sudianto, R. Thinakaran, F. Umam, F. Adiputra, Izzuddin, and R. S. Debora, "Optimizing K-nearest neighbors with particle swarm optimization for improved classification accuracy," *Jurnal Ilmiah Teknik Elektro Komputer dan Informatika (JITEKI)*, vol. 11, no. 2, pp. 238–250, 2025, https://journal.uad.ac.id/index.php/JITEKI/article/view/30775.

[42] M. A. Al-Ali, O. F. Lutfy, and H. Al-Khazraji, "Investigation of optimal controllers on dynamic performance of nonlinear active suspension systems with actuator saturation," *Journal of Robotics and Control (JRC)*, vol. 5, no. 4, pp. 1041–1049, 2024, https://journal.umy.ac.id/index.php/jrc/article/view/22139.

[43] Z. Jin, X. Sun, G. Lei, Y. Guo, and J. Zhu, "Sliding mode direct torque control of SPMSMs based on a hybrid wolf optimization algorithm," *IEEE Transactions on Industrial Electronics*, vol. 69, no. 5, pp. 4534–4544, 2022, https://doi.org/10.1109/TIE.2021.3080220.

[44] M. R. Abd-Elwahab, M. M. Makrahy, M. N. Ghazaly, and A. O. Moaaz, "Optimization and analysis of the quarter car passive suspension using Taguchi, genetic algorithm, and simulated annealing approaches," *International Journal of Transport Development and Integration*, vol. 8, no. 3, pp. 383–392, 2024, https://doi.org/10.18280/ijtdi.080302.

[45] V. C. Bui, V. Q. Le, A. N. Ngo, and C. H. Canh, "Firefly algorithm-based PID optimization for active suspension systems in electric vehicles," *Journal of Fuzzy Systems and Control*, vol. 3, no. 2, pp. 142–148, 2025, https://ejournal.ptti.web.id/index.php/jfsc/article/view/311.

[46] F. R. Yaseen and H. Al-Khazraji, "Optimized vector control using swarm bipolar algorithm for five-level PWM inverter-fed three-phase induction motor," *International Journal of Robotics and Control Systems*, vol. 5, no. 1, pp. 333–347, 2025, https://doi.org/10.31763/ijrcs.v5i1.1713.

[47] H. S. Dakheel, Z. B. Abdullah, and S. W. Shneen, "Advanced optimal GA-PID controller for BLDC motor," *Bulletin of Electrical Engineering and Informatics*, vol. 12, no. 4, pp. 2077–2086, 2023, https://doi.org/10.11591/beei.v12i4.4649.

[48] P. Chotikunnan, W. Khotakham, A. Wongkamhang, A. Nirapai, P. Imura, K. Roongpraser, R. Chotikunnan, and N. Thongpance, "Genetic algorithm-optimized LQR for enhanced stability in self-balancing wheelchair systems," *Control Systems and Optimization Letters*, vol. 2, no. 3, pp. 327–335, 2024, https://doi.org/10.59247/csol.v2i3.161.

[49] A. A. Flaih, E. H. Karam, and Y. A. Mohammed, "Optimal PID controller based on modified grasshopper optimization algorithm for nonlinear single-input single-output system," *Buletin Ilmiah Sarjana Teknik Elektro*, vol. 7, no. 4, pp. 756–773, 2025, https://garuda.kemdiktisaintek.go.id/documents/detail/5571009.

[50] M. J. Mohamed and L. T. Rasheed, "Design of nonlinear PID and FOPID controllers for electronic throttle valve position," *Journal of Electrical and Computer Engineering*, vol. 2024, p. 9984750, 2024, https://doi.org/10.1155/2024/9984750.

[51] R. S. Hassan and F. R. Yaseen, "Sensorless speed control for PMSM based on multi-level SVPWM inverter and MRAS," *Iraqi Journal of Computers, Communications, Control and Systems Engineering*, vol. 23, no. 2, pp. 37–50, 2023, https://doi.org/10.33103/uot.ijccce.23.2.4.

[52] M. Hamzah, L. Majeed, A. S. Al-Araji, H. Dulaimi, and H. Al-Khazraji, "Sliding mode control based whale optimization algorithm for Duffing oscillator," *International Journal of Robotics and Control Systems*, vol. 6, no. 1, pp. 495–506, 2026, https://pubs2.ascee.org/index.php/IJRCS/article/view/2451.

[53] A. A. Abdelhamid, S. K. Towfek, N. Khodadadi, A. A. Alhussan, D. S. Khafaga, M. M. Eid, and A. Ibrahim, "Waterwheel plant algorithm: A novel metaheuristic optimization method," *Processes*, vol. 11, no. 5, p. 1502, 2023, https://doi.org/10.3390/pr11051502.

[54] S. Poppinga, J. Smaij, A. S. Westermeier, M. Horstmann, S. Kruppert, R. Tollrian, and T. Speck, "Prey capture analyses in the carnivorous aquatic waterwheel plant (*Aldrovanda vesiculosa* L., Droseraceae)," *Scientific Reports*, vol. 9, no. 1, p. 18590, 2019, https://doi.org/10.1038/s41598-019-54857-w.

[55] A. A. Alhussan, A. A. Abdelhamid, E. S. M. El-Kenawy, A. Ibrahim, M. M. Eid, D. S. Khafaga, and A. E. Ahmed, "A binary waterwheel plant optimization algorithm for feature selection," *IEEE Access*, vol. 11, pp. 94227–94251, 2023, https://doi.org/10.1109/ACCESS.2023.3312022.

[56] D. S. Khafaga, N. Khodadadi, E. Khodadadi, A. A. Alhussan, M. M. Eid, and E. M. El-Kenawy, "Enhanced early chronic kidney disease prediction using hybrid waterwheel plant algorithm for deep neural network optimization," *Scientific Reports*, vol. 15, no. 1, p. 42584, 2025, https://doi.org/10.1038/s41598-025-26382-6.

[57] S. Askar, S. Uma, G. Sethi, M. S. Ramkumar, and S. Dhivya, "Smart grid stability enhancement using waterwheel plant algorithm for demand side management," in *2025 7th International Conference on Inventive Material Science and Applications (ICIMA)*, 2025, pp. 379–385, https://doi.org/10.1109/ICIMA64861.2025.11073955.

[58] M. A. E. Mohamed, K. Jagatheesan, and B. Anand, "Modern PID/FOPID controllers for frequency regulation of interconnected power systems considering different cost functions," *Scientific Reports*, vol. 13, no. 1, p. 14084, 2023, https://doi.org/10.1038/s41598-023-41024-5.

[59] P. Anbarasu, N. Loganathan, A. Narendran, and K. Rameshkumar, "Design and intelligent tuning of a proportional-integral-derivative controller for an armature-controlled DC motor," *International Journal of Advanced Technology and Engineering Exploration*, vol. 13, no. 134, pp. 85–101, 2026, https://doi.org/10.19101/IJATEE.2025.121220008.

[60] S. Salim, M. Rahmat, L. Abdullah, S. Shamsudin, K. Kamaludin, and M. Ibrahim, "Comparative insights into nonlinear PID-based controller design approaches for industrial applications," *IAES International Journal of Robotics and Automation*, vol. 14, no. 2, pp. 191–203, 2025, https://doi.org/10.11591/ijra.v14i2.pp191-203.